

Verification of Polarization Reversal of Electromagnetic Waves with Electron Cyclotron Frequency Controlling Plasma-Structure Formation

Toshiro KANEKO, Kazunori TAKAHASHI^{a)} and Rikizo HATAKEYAMA

Department of Electronic Engineering, Tohoku University, Sendai 980-8579, Japan

(Received 17 February 2007 / Accepted 27 June 2007)

Selectively launched electromagnetic waves with left- and right-handed polarizations for $m = 0, +1$, and -1 modes are investigated in terms of polarization reversal around an electron cyclotron resonance (ECR) region in inhomogeneously magnetized plasmas, where m is an azimuthal mode number. It is observed for the first time that a left-handed polarized wave for $m = 0$ mode is absorbed near the ECR point as a result of the polarization reversal in the axial direction. Dispersion analysis in bounded plasmas can explain this quantitatively. For $m = +1$ and -1 modes, on the other hand, polarization reversal occurs along the radial axis, i.e., wave polarization for $m = +1$ mode is right-handed (left-handed for $m = -1$ mode) around the central area and left-handed (right-handed for $m = -1$ mode) around the peripheral area of the cross section of the plasma column. Furthermore, we investigate plasma-potential structures formed by ECR of high-power $m = +1$ and -1 waves and, for the first time, demonstrate control of the plasma-potential structure by changing the azimuthal mode, i.e., a positive potential hill is formed near the ECR point around the central and peripheral areas for $m = +1$ and -1 modes, respectively.

© 2007 The Japan Society of Plasma Science and Nuclear Fusion Research

Keywords: electron cyclotron wave, polarization reversal, structure formation, magnetized plasma

DOI: 10.1585/pfr.2.038

1. Introduction

It is of crucial importance to clarify the characteristics of electromagnetic wave propagation and absorption in magnetized plasmas, because the waves exhibit interesting physics and afford possibilities for wide-range applications. In particular, the electromagnetic waves with an electron cyclotron resonance (ECR) frequency have attractive characteristics for realizing a thermonuclear fusion, for generating high-energy relativistic electrons in the Earth's magnetosphere, as plasma sources for plasma processing, and so on. In the field of the thermonuclear fusion, ECR is indispensable for efficient electron heating [1] and forming a local-confining potential structure in tandem-mirror devices [2–4]. The generation and propagation of whistler mode waves in the Earth's magnetosphere is an important research subject in magnetospheric physics, and the generation mechanisms of very low frequency (VLF) triggered emission [5, 6] and whistler mode chorus emission [7] have been investigated recently. The resonant scattering process via the electromagnetic whistler mode wave is a candidate for the acceleration mechanism of the relativistic electrons in inner magnetosphere [8]. On the other hand, ECR is effective for producing plasmas with high density, large diameter, lower electron temperature, and a uniform density

profile in the field of processing plasmas [9–12]. It is obvious that the wave propagation and absorption determine the heating efficiency and characteristics of the produced plasma.

Over the past few decades, a considerable number of studies have focused on the whistler wave for weakly magnetized plasmas ($\omega_{pe}/\omega_{ce} > 1$) [13–19] because the wave has right-handed polarization and is efficiently absorbed near the ECR point, where $\omega_{pe}/2\pi$ and $\omega_{ce}/2\pi$ are the electron-plasma and electron-cyclotron frequencies, respectively. On the other hand, wave propagation and absorption under the condition of $\omega_{pe}/\omega_{ce} < 1$ have been investigated recently to produce uniform plasmas [20, 21], in which a left-hand polarized wave (LHPW) is locally absorbed near the ECR point in inhomogeneously magnetized plasmas. To explain the unexpected absorption of the LHPW, which is not considered to be related to ECR, polarization reversal from the LHPW to a right-hand polarized wave (RHPW) was suggested for $m = -1$ mode by theoretical studies including the effects of radial boundaries and finite electron temperature [22]. Here, m is an azimuthal mode number and it was argued that wave polarization changes along the radial axis, i.e., the polarization becomes right-handed in some radial region. Although an experiment on the polarization reversal was performed in an ECR discharge [20], it did not provide clear-cut experimental results because the waves were used for both

author's e-mail: kaneko@ecei.tohoku.ac.jp

^{a)} Present address: Department of Electrical and Electronic Engineering, Iwate University, Morioka 020-8551, Japan

studying the wave propagation and producing the plasma. Here, we claim that, to avoid nonlinear effects, it is necessary to selectively launch the small-amplitude RHPW or LHPW into a steady-state plasma, pre-produced by a direct current (DC) discharge [23–25]. Besides, theoretical and numerical analyses should be performed for clarifying the effects of the boundaries in plasma-filled waveguides [26–29] on the wave propagation and the unexpected absorption of the LHPW through the polarization reversal near the ECR point.

This polarization reversal is investigated initially on Alfvén waves in the range of the ion cyclotron frequency [30, 31], where the wave polarization reverses from right-handed ($m = +1$ mode) to left-handed ($m = -1$ mode). The ions are heated effectively by these converted waves. However, there are few experimental results on electron heating resulting from the polarization reversal in the range of the electron cyclotron frequency.

With this background, the present work intends to interpret the propagation and damping phenomena of the LHPW near the ECR point from the viewpoint of the radial boundary effects, and to demonstrate modifications of the plasma structure, such as electron-temperature and plasma-potential profiles, resulting from the polarization reversal. In this paper, we report the difference in the propagation and absorption mechanisms between microwaves with an axisymmetric $m = 0$ mode [32–34] and nonaxisymmetric $m = +1$ and -1 modes [34]. In addition, we discuss the characteristics of the polarization reversals theoretically and their effects on controlling the plasma-structure formation for $m = +1$ and -1 modes.

2. Theoretical Dispersion Relation in Bounded Plasmas

We consider an azimuthally and radially uniform plasma column, because the radial profile of electron density is almost uniform in our experiments. A dielectric tensor \mathbf{K} in cold plasmas is given by

$$\frac{\omega^2}{c^2} \mathbf{K} = \begin{pmatrix} \kappa_1 & \kappa_2 & 0 \\ -\kappa_2 & \kappa_1 & 0 \\ 0 & 0 & \kappa_3 \end{pmatrix}, \quad (1)$$

with κ_1 , κ_2 , and κ_3 defined by

$$\begin{aligned} \frac{c^2}{\omega^2} \kappa_1 &= 1 - \sum_j \frac{\omega_{pj}^2}{\omega^2 - \omega_{cj}^2}, \\ i \frac{c^2}{\omega^2} \kappa_2 &= \sum_j \frac{\epsilon_j \omega_{cj} \omega_{pj}^2}{\omega(\omega^2 - \omega_{cj}^2)}, \\ \frac{c^2}{\omega^2} \kappa_3 &= 1 - \sum_j \frac{\omega_{pj}^2}{\omega^2}, \end{aligned}$$

where $\omega_{pj}/2\pi$, $\omega_{cj}/2\pi$, and ϵ_j are the plasma frequency, the cyclotron frequency, and the sign of the charge for species j . The terms related to ion motions can be neglected in the

case of $\omega \gg \omega_{pi}$, ω_{ci} , where $\omega_{pi}/2\pi$ and $\omega_{ci}/2\pi$ are the ion-plasma and ion-cyclotron frequencies. A dispersion relation of electromagnetic waves in bounded plasmas is derived from the Maxwell equations as [35]

$$(\gamma^2 + \kappa_2^2 + \gamma k_\perp^2) \kappa_3 + k_\perp^2 [\kappa_1(\gamma + k_\perp^2) - \kappa_2^2] = 0, \quad (2)$$

where $\gamma \equiv k_\parallel^2 - \kappa_1$, and k_\parallel and k_\perp are the wave numbers parallel and perpendicular to a static magnetic field \mathbf{B} in the z -direction, respectively. The electric fields are assumed to propagate in the z -direction, therefore, wave fields with azimuthal mode number m can be represented by

$$\mathbf{E} = \mathbf{E}(r) \exp[i(k_\parallel z + m\theta - \omega t)], \quad (3)$$

where the components of the electric-field vector are derived as

$$E_z(r) = \frac{\omega \kappa_1 \beta A}{k_\parallel \kappa_2 \kappa_3} J_m(k_\perp r), \quad (4)$$

$$E_r(r) = \frac{i\omega \delta A}{\kappa_2 k_\perp} J'_m(k_\perp r) - \frac{m\omega A}{r k_\perp^2} J_m(k_\perp r), \quad (5)$$

$$E_\theta(r) = -\frac{m\omega \delta A}{r \kappa_2 k_\perp^2} J_m(k_\perp r) - \frac{i\omega A}{k_\perp} J'_m(k_\perp r), \quad (6)$$

where $\beta \equiv \gamma - \kappa_2^2/\kappa_1 + k_\perp^2$, $\delta \equiv \gamma + k_\perp^2$, and A and J_m are an amplitude constant and the Bessel function of order m , respectively. Here, E_r and E_θ (in cylindrical coordinates) correspond to experimentally obtained E_x and E_y (in rectangular coordinates). In a plasma-filled waveguide with a diameter comparable to the wavelength of the electromagnetic wave, the perpendicular wave number k_\perp is determined by radial boundary conditions. Although the parallel wave number k_\parallel is also affected by axial boundary conditions, the parallel wavelength is much less than the axial length of the plasma column in our experimental configurations, therefore, its effects can be neglected.

The wave polarization plays important roles in the cyclotron resonance phenomena. The above dispersion relation and electric-field components derive a polarization index S as

$$S \equiv \frac{|E_r + iE_\theta|}{|E_r - iE_\theta|}. \quad (7)$$

Here, $0 < S < 1$ and $1 < S < \infty$ represent right- and left-handed polarizations, and $S = 0$, $S = 1$, and $S = \infty$ correspond to circularly right-handed, linear, and circularly left-handed polarizations, respectively. The wave polarization can become both right- and left-handed following Eq. (7), which is determined by Eqs. (5) and (6), derived from the solution of Eq. (2), and depends on the plasma parameters such as electron density and magnetic-field strength.

3. Experiments on Axisymmetric Mode

3.1 Experimental apparatus

Experiments are performed in the Q_T-Upgrade Machine of Tohoku University, shown in Fig. 1, which is a

linear device with vacuum chamber about 450 cm in length and 20.8 cm in diameter. The inhomogeneous magnetic field B presented at the bottom of Fig. 1 is applied by two parties of solenoidal coils. The magnetic field B is altered to vary the characteristic length L_B of magnetic-field gradient, which is defined as $L_B = [(1/B)dB/dz]^{-1}$. A coaxially bounded plasma with outer vacuum layer is produced by a DC discharge between a barium oxide (BaO) cathode and a tungsten-mesh anode in low pressure argon gas (90 mPa). The plasma column is terminated with a glass endplate located on the opposite side of the plasma source. A clear boundary is formed between the plasma and the vacuum layer using a limiter, which is located just in front of the tungsten-mesh anode. It also controls the plasma radius r_p in the range of 2.5-4 cm. Langmuir probes, movable in radial and axial directions, are set to measure plasma parameters and their radial and axial profiles. The typical electron density and temperature at the radial center of the plasma column are $n_e \approx 9 \times 10^{10} \text{ cm}^{-3}$ and $T_e = 3 \text{ eV}$ at $z = 78 \text{ cm}$, where $z = 0 \text{ cm}$ is defined as the axial position of a microwave exciter (described below).

A microwave (frequency: $\omega/2\pi = 6 \text{ GHz}$, power: $P_{\text{in}} = 150 \text{ mW}$) is excited as an axisymmetric $m = 0$ mode in the high magnetic-field region by a helical antenna ($z = 0 \text{ cm}$), and launched toward the ECR point ($B = 2.14 \text{ kG}$, $z = 78 \text{ cm}$) satisfying the condition of $\omega/\omega_{ce} < 1$. The helical antenna is designed to operate at 6 GHz, according to the theory in Ref. [36]. The helix diameter, the axial length, the number of turns, and the diameter of the ground plane behind the helix are 1.6 cm, 12 cm, 10 turns, and 3.75 cm, respectively. This helical antenna can selectively launch the RHPW or LHPW when the magnetic-field direction, or the electron Larmor-rotation direction is changed [23]. We define the terms ‘‘R-mode excitation’’ and ‘‘L-mode excitation’’ as the excitation modes where the wave electric-field E rotates in the directions same as and opposite to the electron rotation, respectively. The wave patterns are obtained with an inter-

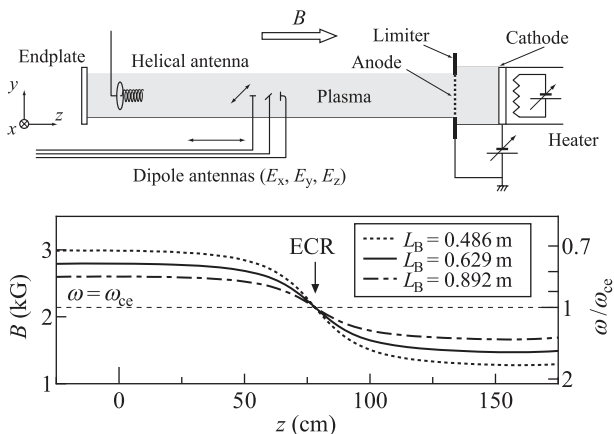


Fig. 1 Schematic of the experimental setup for axisymmetric mode and external static magnetic-field configuration.

ference method using a mixer through movable balanced dipole antennas with folded balun, which can receive each component of wave electric field, i.e., E_x , E_y , and E_z , respectively, and are terminated with 50Ω lines. The antennas are covered with ceramics to protect them from thermal damage. The dipole length is 1.8 cm, as this provides maximum sensitivity. Shifting the phase of the received signal using a phase shifter inserted between the dipole antennas and the mixer, provides time-series measurements of the electric field, because the interferometric wave pattern is a snapshot of the electric-field structure at a certain time.

3.2 Experimental results and discussion

Figure 2 shows interferometric wave patterns of E_y at the radial center of the plasma column for (a) R-mode and (b) L-mode excitations in the inhomogeneous magnetic field with $L_B = 0.892 \text{ m}$ (solid arrows at $z = 78 \text{ cm}$ indicate the position of ECR point of the 6 GHz microwave). The wavelengths of R-mode and L-mode excitations are shorter and longer compared with the wavelengths in vacuum, therefore, they correspond to the RHPW and LHPW, respectively [23]. This demonstrates that the helical antenna can selectively excite the RHPW or LHPW by changing the magnetic-field direction. The interferometric wave pattern for R-mode excitation [Fig. 2 (a)] shows that the wavelength becomes gradually shorter and the amplitude decreases steeply as the wave reaches the ECR point. The interferometric wave pattern for L-mode excitation [Fig. 2 (b)], on the other hand, demonstrates that the long wavelength wave propagates and disappears near the ECR point in the same way as the RHPW. We confirmed these waves are not standing waves but traveling waves. These observations give the possibility for the absorption of the LHPW in the ECR region. To interpret this unexpected

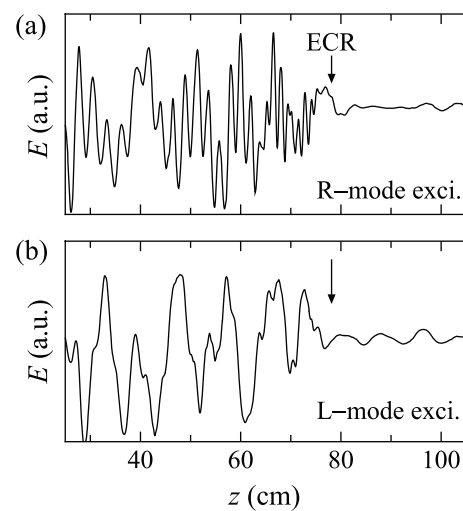


Fig. 2 Interferometric wave pattern of E_y observed at the radial center of the plasma column for (a) R-mode and (b) L-mode excitations in the inhomogeneous magnetic field with $L_B = 0.892 \text{ m}$.

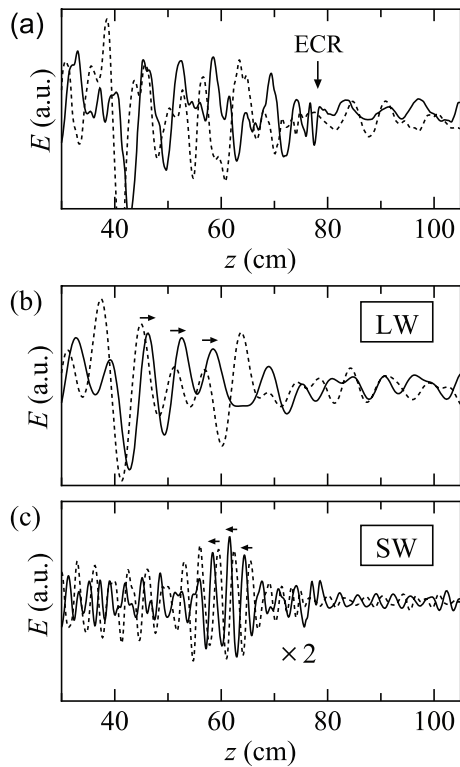


Fig. 3 (a) Interferometric wave patterns of E_x (dashed line) and E_y (solid line) observed at the radial center of the plasma column for $L_B = 0.629$ m. (b) Long (LW) and (c) short (SW) wavelength components decomposed from the wave patterns in Fig. 3 (a) by Fourier analysis.

LHPW absorption, we concentrate on L-mode excitation.

Figure 3 (a) shows interferometric wave patterns of E_x (dashed line) and E_y (solid line) in L-mode excitation for $L_B = 0.629$ m, which indicate damping of the launched wave near the ECR point similar to that shown in Fig. 2 (b). Note that, in Fig. 3 (a), the wave patterns include both the long (LW) and short (SW) wavelength components. Figures 3 (b) and 3 (c) present the LW and SW components, respectively, decomposed from the wave patterns in Fig. 3 (a) by Fourier analysis. The LW damps and the SW grows around $z = 60$ cm, and the phase differences of E_x to E_y for the LW and SW indicated by arrows in Figs. 3 (b) and 3 (c), are shifted in opposite direction. These phase differences (between E_x and E_y) identify the LW and SW as the LHPW and RHPW, respectively.

We also show the electric-field vector of the LW at $z = 53$ cm and the SW at $z = 70$ cm for $L_B = 0.486$ m depending on time. These results are obtained from the wave patterns of E_x and E_y by shifting the phase of the received signal, and are plotted in Figs. 4 (a) and 4 (b), respectively. Here, the numbers in closed marks denote the time at intervals of $T/8$, where the symbol T is the period of the 6 GHz microwave and the solid lines with arrows denote the rotational direction of the observed vector. The LW and SW polarizations are left- and right-handed, respectively [33]. Therefore, clearly, the LHPW is gradually converted into

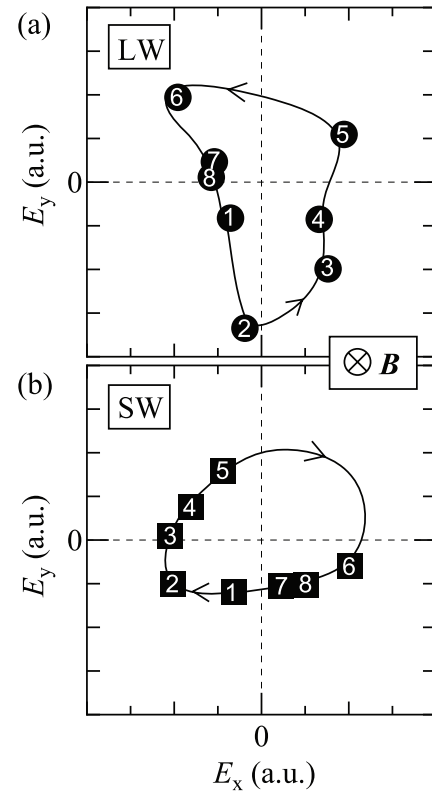


Fig. 4 Time-series of the electric-field vector in the transverse plane against the magnetic-field lines of (a) the LW at $z = 53$ cm and (b) the SW at $z = 70$ cm for $L_B = 0.486$ m.

the RHPW before the ECR point, that is, the polarization reversal occurs from the LHPW to the RHPW, and as a result, the launched LHPW is absorbed near the ECR point.

For characterizing the polarization reversal, the RHPW component, decomposed from the observed wave patterns of E_y for $L_B = 0.486, 0.578,$ and 0.713 m, is presented in Fig. 5 (a) for $r_p = 3$ cm. To estimate the polarization reversal point, we define z_{pr} as an axial point where the RHPW has maximum amplitude, indicated by arrows in Fig. 5 (a). z_{pr} shifts gradually to the upper region of propagation as L_B increases. Figure 5 (b) shows the magnetic-field strength B_{pr} at the polarization reversal point $z = z_{pr}$ as a function of L_B . Since we expect the radial boundary to cause these phenomena, the dependencies of B_{pr} on L_B are also measured with changes in the plasma radius r_p . The value of B_{pr} is almost constant with respect to L_B for each plasma radius. This indicates that the polarization reversal from the LHPW to the RHPW occurs when B attains a certain value. In addition, the value of B_{pr} becomes large with an increase in r_p . The polarization reversal point is dominated by the plasma radius, i.e., the radial boundary condition between the plasma and the vacuum regions [32].

We compare the experimental results with the dispersion theory described in Sec. 2. The experimentally observed radial profile of E_z describes that $m = 0$ mode is formed under our experimental condition, and the perpendicular wave number is $k_{\perp} = 1.15$ cm $^{-1}$ at $z = 40$ cm

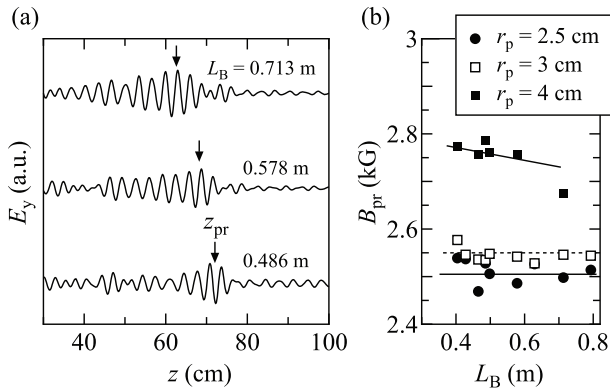


Fig. 5 (a) RHPW component decomposed from the observed wave pattern of E_y for $r_p = 3$ cm and each characteristics length L_B . (b) Dependence of the magnetic field B_{pr} at the polarization reversal point on L_B for each plasma radius r_p .

for $r_p = 3$ cm. In addition, the effects of the inhomogeneous magnetic-field configuration on n_e and k_{\perp} , i.e., the inhomogeneous axial profiles of n_e and k_{\perp} are taken into account in calculating the dispersion relation with B as a variable. Figure 6(a) shows the calculated dispersion relation as a solid line, along with the experimental dispersion relations obtained from the LHPW (closed square) and the RHPW (open square) components, i.e., the LW in the high magnetic-field region and the SW growing near the ECR point (Fig. 3). The calculated dispersion curve is in good agreement with the experimental ones. The polarization index S in Eq. (7) is also plotted in Fig. 6(b) for theoretical verification of the experimentally observed polarization reversal from the LHPW to the RHPW. The value of S for $r_p = 3$ cm is larger than unity in the range of $\omega/\omega_{ce} < 0.85$, i.e., the wave polarization is left-handed. As the wave approaches the ECR point ($\omega/\omega_{ce} = 1$), the value of S become smaller than unity. Therefore, the polarization reversal from the LHPW to the RHPW theoretically occurs through a linear polarized wave on the condition of $\omega/\omega_{ce} = 0.85$, which can well explain the experimental results. The launched LHPW is efficiently absorbed by ECR, because the wave polarization becomes right-handed, obeying the dispersion relation including the effects of the radial boundary, i.e., a perpendicular wave number. Moreover, the polarization index shows the same value at any radial position in the plasma region for $m = 0$. The polarization reversal occurs simultaneously over the entire cross section of the plasma column [34].

To interpret the change of the polarization reversal point with an increase in r_p as shown in Fig. 5 (b), the polarization index is calculated for each plasma radius r_p . Since the experimentally observed radial profiles of E_z give $k_{\perp} = 1.2, 1.15$, and 1.1 cm^{-1} for $r_p = 2.5, 3$, and 4 cm, respectively, the polarization index S can be calculated using these values of k_{\perp} for each r_p as shown in Fig. 6 (b). The polarization reversal points correspond to ω/ω_{ce} at $S = 1$

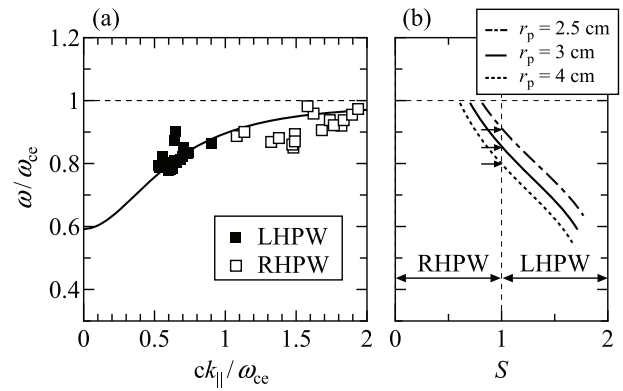


Fig. 6 (a) Calculated dispersion relation for $k_{\perp} = 1.15$ cm^{-1} , together with experimental dispersion relations obtained from the LHPW (closed square) and the RHPW (open square) for $r_p = 3$ cm. (b) Calculated polarization index S corresponding to the dispersion curve with r_p as a parameter.

on the calculated curves, which are indicated by arrows in Fig. 6 (b). The calculated ω/ω_{ce} at $S = 1$ becomes smaller with an increase in r_p , i.e., a decrease in k_{\perp} . The magnetic-field strength corresponding to ω/ω_{ce} at $S = 1$ for $r_p = 2.5, 3$, and 4 cm are 2.35, 2.52, and 2.68 kG, respectively. These values are almost consistent with the experimental results observed in Fig. 5 (b). Therefore, this proves that the polarization reversal point from the LHPW to the RHPW is determined by the dispersion relation including the effects of the radial boundary, dominating the perpendicular wave number k_{\perp} . For $r_p = 2.5$ cm, the experimentally obtained polarization reversal point shifts slightly to the high magnetic-field side compared with the theoretical polarization reversal point. Since the polarization reversal point is close to the ECR point ($\omega/\omega_{ce} = 0.91$ at $z = z_{pr}$) for $r_p = 2.5$ cm, the wave starts to damp before the LHPW entirely converts to the RHPW. Therefore, the polarization reversal point, which is determined as the axial point where the RHPW has the maximum amplitude, seems to shift to the point where ECR absorption starts.

4. Experiments on Nonaxisymmetric Mode

4.1 Experimental apparatus

Experiments on the nonaxisymmetric mode are performed on the same machine as for the axisymmetric mode. Here, we adopt the converging magnetic-field configuration presented in Fig. 7. In this case, microwaves (frequency: $\omega/2\pi = 6$ GHz, power: $P_{in} = 0 - 50$ W) with $m = +1$ and -1 modes are selectively launched from the high magnetic-field side using a horn antenna with a dielectric polarizer [37, 38]. In addition, a novel plasma source for controlling the field-aligned ion-flow energy under low argon gas pressures (~ 10 mPa) is set at the low magnetic-field side. The anode potential V_a controls the ion flow energy [39, 40]. The plasma column is terminated

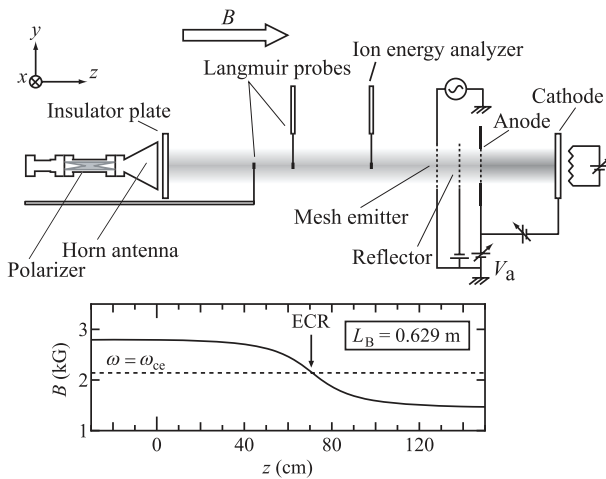


Fig. 7 Schematic of the experimental setup for nonaxisymmetric mode and external static magnetic-field configuration.

with an insulator plate in front of the horn antenna, and its radius is limited to about 3 cm by a limiter located at the same position as the anode. The ECR point of the 6 GHz microwave is $z = 71$ cm, where $z = 0$ is defined as an axial position of the front of the horn antenna, as indicated in Fig. 7. A Langmuir probe and dipole antennas measure the spatial profiles of plasma parameters and the electric fields E_x , E_y , and E_z of the microwaves in the same way as for the axisymmetric mode experiments. A network analyzer provides spatial profiles of wave phase.

For the nonaxisymmetric mode, the relationship between the sign of the mode ($m = +1$ and -1) defined as a global-rotation direction determined by the geometric structure of the excitation antenna and the polarization (RHPW and LHPW) defined as a local-rotation direction at each position in the vacuum chamber acting as a waveguide, is significant and is discussed later.

4.2 Experimental results and discussion

Figure 8 shows interferometric wave patterns at the radial center of the plasma column for (a) $m = +1$ and (b) $m = -1$ modes. Solid arrows at $z = 71$ cm indicate the ECR point. The interferometric wave pattern for $m = +1$ mode demonstrates that the wave amplitude steeply decreases around the ECR point, i.e., the wave is damped because of the ECR absorption. However, the wave amplitude again increases in the weak magnetic-field side from the ECR point. Since a part of the wave propagates in the outer vacuum region and passes through the ECR point without absorption, the wave is reflected at the anode and again propagates toward the ECR point from the weak magnetic-field side. For $m = -1$ mode, the interferometric wave pattern shows that the wave is not absorbed around the ECR point. This implies that the polarization for $m = -1$ mode is left-handed at the radial center and the polarization reversal does not occur unlike the case of

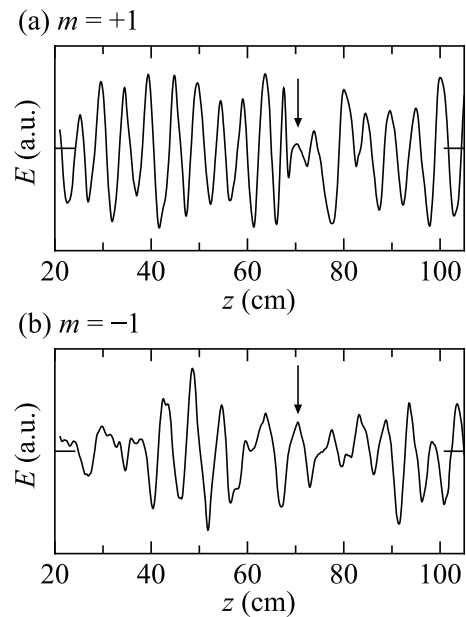


Fig. 8 Interferometric wave patterns of E_x for $P_{in} = 150$ mW of (a) $m = +1$ mode and (b) $m = -1$ mode observed at the radial center of the plasma column.

LHPW for $m = 0$ mode.

Interpreting the above-mentioned difference in the wave absorption between $m = +1$ and -1 modes, requires understanding the related characteristics of the electromagnetic waves. Figure 9 plots the radial (x) profiles of the phase difference $\Delta\theta$ between E_x and E_y of the microwave electric fields at $z = 60$ cm as $\sin \Delta\theta$ (open circles) for (a) $m = +1$ and (b) $m = -1$ modes, where the right- and left-handed polarizations are represented by $-1 < \sin \Delta\theta < 0$ and $0 < \sin \Delta\theta < +1$, respectively. The shaded areas indicate the experimentally obtained right-handed polarization regions. Polarization for $m = +1$ mode is right-handed in the central area and left-handed around the peripheral area, i.e., the polarization reverses along the radial axis. In contrast, for $m = -1$ mode, the right- and left-handed polarizations are observed around the peripheral and central areas, respectively, as plotted in Fig. 9 (b). As described in Sec. 1, the polarization of the Alfvén waves of $m = +1$ and -1 modes reverses along the radial axis. The same phenomenon is for the first time observed in the range of the ECR frequency.

For explaining the experimental results on the polarization profiles, Fig. 9 shows the theoretical polarization index S for $m = +1$ and -1 modes, transformed into $\sin \Delta\theta [= (S - 1)/(S + 1)]$ and presented as solid lines. In the calculation of $\Delta\theta$, the parameters of $k_{\perp} = 1.02$ and 1.20 cm^{-1} are used for $m = +1$ and -1 modes, respectively, according to the measured results of radial E_z -profiles denoting the excitation of $m = +1$ and -1 modes. The theoretical $\Delta\theta$ shows that the wave polarization for $m = +1$ mode is right-handed (left-handed for $m = -1$ mode) in the central area and left-handed (right-handed for $m = -1$

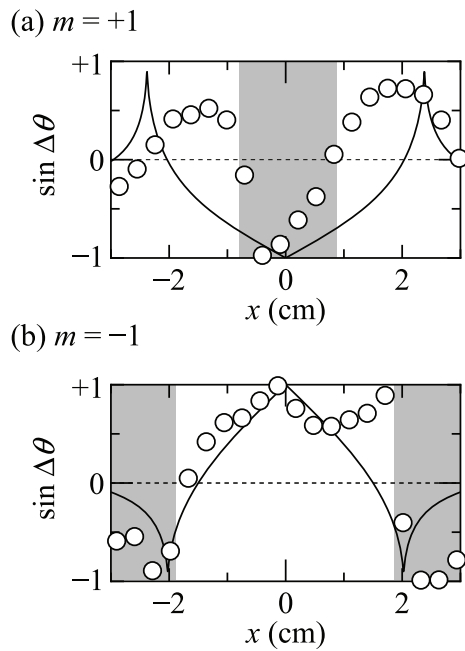


Fig. 9 Radial (x) profiles of the experimentally obtained phase difference $\Delta\theta$ (open circles) between E_x and E_y of the microwaves, and the theoretical polarization index S (solid lines) which is transformed into $\Delta\theta [= \arcsin(S - 1)/(S + 1)]$ for (a) $m = +1$ mode and (b) $m = -1$ mode at $z = 60$ cm. The phase difference $\Delta\theta$ is plotted as $\sin \Delta\theta$ and the shaded areas indicate the experimentally obtained right-handed polarization regions ($-1 < \sin \Delta\theta < 0$).

mode) around the peripheral area. Therefore, the experimentally observed polarization profiles are well explained by the dispersion theory in bounded plasmas.

To clarify how the polarization is changed in the radial direction, we theoretically calculate the spatial structure of the microwave electric-fields using the dispersion relation with the boundary condition. Figure 10 presents a time-series of the calculated electric-field vector in transverse planes against the magnetic-field lines for (a) $m = +1$ and (b) $m = -1$ modes, where the symbol T is the period of the microwave. For $m = +1$ mode, the global structure of the electric-field vector rotates right-handed, which means the sign of the mode is positive. When we concentrate on the local-rotation direction (polarization), the electric-field vector clearly rotates right-handed (RHPW) at the radial center and left-handed (LHPW) in the peripheral area. For $m = -1$ mode, on the other hand, the excited wave is the LHPW in the central area and the RHPW around the peripheral area. This behavior is entirely opposite to that of $m = +1$ mode. These results reveal that the local-rotation direction (the polarization) at the radial center is the same as the global-rotation direction (the sign of the mode), and changes to the opposite direction in the peripheral area as a consequence of the polarization reversal in the radial direction. We observed in Fig. 8 that the microwave is absorbed in the central area for $m = +1$ mode, whereas the wave for $m = -1$ mode penetrates to ECR point without damp-

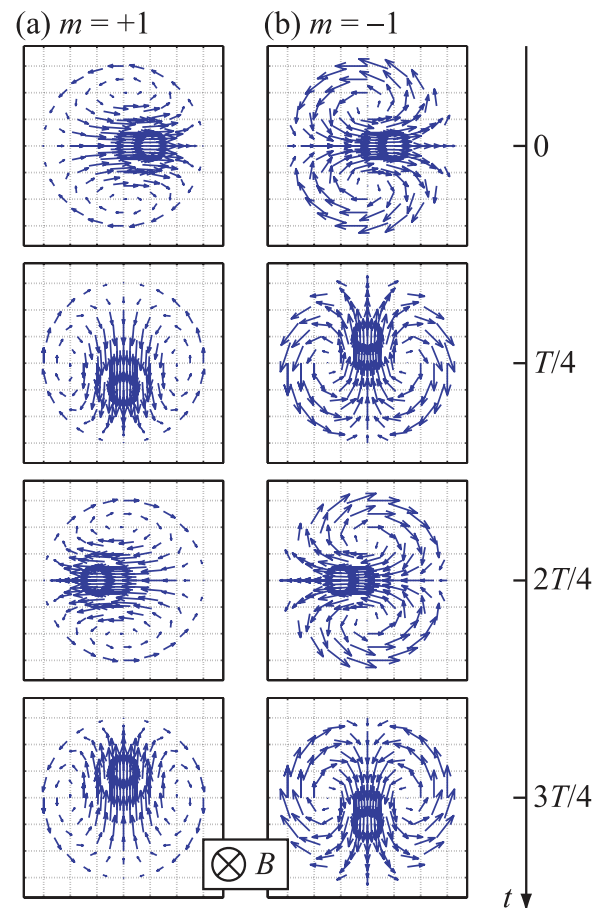


Fig. 10 Temporal evolution of wave electric-field vector for (a) $m = +1$ mode and (b) $m = -1$ mode calculated by the theoretical dispersion relation.

ing. This verifies that the microwave is absorbed around the area where the polarization is right-handed, which is controlled by changing the sign of the azimuthal mode.

This controlled absorption of the microwave could cause spatially selective electron heating, which is expected to be useful for plasma-structure control by microwave-antenna operation. To demonstrate the possibility of plasma-structure control, the plasma parameters are measured while changing the azimuthal mode of the microwaves. Figure 11 gives radial x profiles of (a) electron temperature T_e and (b) space potential ϕ_s for $P_{in} = 0$ W (gray marks), $P_{in} = 50$ W of $m = +1$ mode (black marks), and $P_{in} = 50$ W of $m = -1$ mode (open marks) at $z = 65$ cm, which is an upper region of propagation from the ECR point, under the condition that the ion-flow energy is about 15 eV. T_e is radially homogeneous for $P_{in} = 0$ W, as shown in Fig. 11 (a). For $P_{in} = 50$ W, T_e increases in the central area of the cross section of the plasma column for $m = +1$ mode. For $m = -1$ mode, however, T_e rises in the peripheral area, rather than the central area. This increase in T_e occurs in the area corresponding to the right-handed polarization of the microwaves, as shown in Fig. 9. On the other hand, ϕ_s also increases in the central area compared

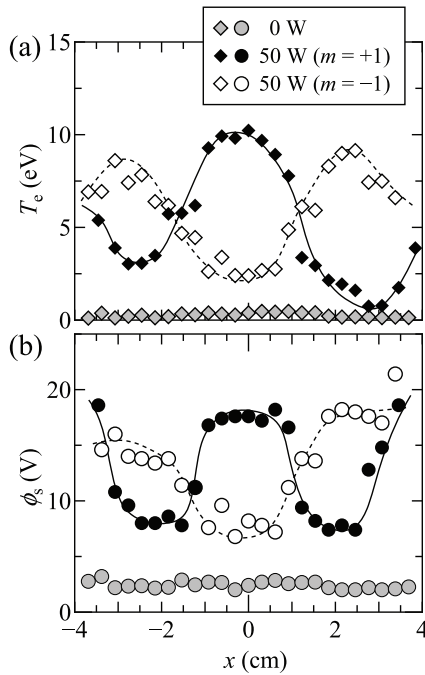


Fig. 11 Radial (x) profiles of (a) electron temperature T_e and (b) space potential ϕ_s at $z = 65$ cm for $P_{in} = 0$ W (gray marks), $P_{in} = 50$ W of $m = +1$ mode (black marks), and $P_{in} = 50$ W of $m = -1$ mode (open marks).

with the peripheral area for $m = +1$ mode, which corresponds to the radial profile of T_e for $m = +1$ mode. For $m = -1$ mode, the radial profile of ϕ_s also has the same tendency as T_e for $m = -1$ mode.

Mechanisms of these potential rises around the ECR region are investigated by measuring the axial z profiles of the space potential ϕ_s , as shown in Fig. 12, for $P_{in} = 50$ W of $m = +1$ mode (closed circles) and $m = -1$ mode (open circles) at (a) $x = 0$ cm and (b) $x = 2$ cm. In the central area ($x = 0$ cm), a drastic positive potential hill appears near the ECR region (≈ 71 cm) for $m = +1$ mode, whereas the potential is almost constant spatially for $m = -1$ mode. In the peripheral area ($x = 2$ cm), on the other hand, the potential hill is formed only for $m = -1$ mode. As already mentioned, the electron temperature increases in the central or peripheral area depending on the sign of the azimuthal mode. Since the electrons heated by the ECR are axially decelerated and reflected by the $-\mu\nabla_{\parallel}B$ force, where μ is the magnetic moment of electrons and $\nabla_{\parallel}B$ is the gradient of B in the direction parallel to magnetic field lines, and ions are not directly affected by the ECR and may pass through the ECR region, the positive potential is expected to be formed to maintain charge neutrality in the high magnetic-field region from the ECR point [3, 4]. Namely, the radial structure of T_e caused by the radially selective heating of the electrons resulting from the polarization reversal in the radial direction, can enhance the plasma-potential structure formation.

These results show that it is possible to control the

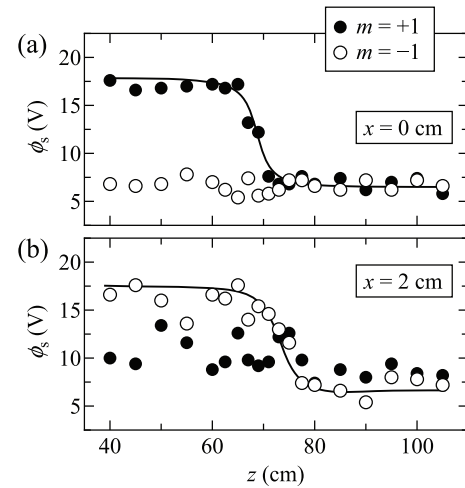


Fig. 12 Axial (z) profiles of space potential for $P_{in} = 50$ W of $m = +1$ mode (closed circles) and $m = -1$ mode (open circles) at (a) $x = 0$ cm and (b) $x = 2$ cm.

potential structure near the ECR point through the variation of the electron temperature just by selecting the azimuthal mode number m of the launched microwave. This spatially controlled plasma potential, i.e., the formation of the axial and radial electric fields by external wave injection, is useful for electrostatic confinement of high-energy ions in tandem-mirror devices [2–4] and the suppression of low-frequency fluctuations [41–43]. Furthermore, we notice that selective electron heating in the peripheral area can be applied to the improvement of the spatial uniformity of the plasma density for plasma processing [9].

5. Conclusions

We investigated the polarization reversal of electromagnetic waves near the electron cyclotron resonance region in inhomogeneously magnetized plasmas for axisymmetric and nonaxisymmetric modes. Experiments on the axisymmetric $m = 0$ mode directly demonstrate, for the first time, the polarization reversal from the LHPW to the RHPW in the axis direction. Dispersion analysis in bounded plasmas provides the theoretical explanation. This polarization reversal yields the efficient and localized absorption of the excited LHPW.

Experiments on the nonaxisymmetric mode, on the other hand, find that the polarization reversal occurs along the radial axis, and the selectively launched microwaves with azimuthal mode numbers $m = +1$ and $m = -1$ propagate as the RHPW in the central and peripheral areas, respectively, and are absorbed in the ECR region. Consequently, the electron temperature increases locally and the plasma-potential structure is formed in the central and peripheral areas, corresponding to the areas of propagation and absorption of the RHPW for $m = +1$ and $m = -1$ modes, respectively. This demonstrates, for the first time, that the plasma-potential structure near the ECR point can

actively be controlled by changing the azimuthal mode of the launched microwave.

Acknowledgments

The authors are indebted to H. Ishida for his technical assistance. We also thank Professor K. Sawaya, Professor A. Fukuyama, Professor M.Y. Tanaka, and Professor Y. Sakawa for their useful comments. The work was supported by a Grant-in-Aid for Scientific Research from the Ministry of Education, Culture, Sports, Science, and Technology, Japan. The work was also supported by the Japan Society for the Promotion of Science for Young Scientists.

- [1] Y. Ikeda, S. Ide, T. Suzuki, A. Kasugai, K. Takahashi, K. Kajiwara, A. Isayama, T. Oikawa, K. Hamamatsu, Y. Kamada, T. Fujita, K. Sakamoto, S. Moriyama, M. Seki, R. Yoshino, T. Imai, K. Ushigusa, T. Fujii and JT-60 Team, *Nucl. Fusion* **42**, 375 (2002).
- [2] T. Cho, H. Higaki, M. Hirata, H. Hojo, M. Ichimura, K. Ishii, A. Itakura, I. Katanuma, J. Kohagura, Y. Nakashima, T. Saito, Y. Tatematsu, M. Yoshikawa, R. Minami, T. Numakura, M. Yoshida, M. Watanabe, K. Yatsu and S. Miyoshi, *Nucl. Fusion* **43**, 293 (2005).
- [3] T. Kaneko, R. Hatakeyama and N. Sato, *Phys. Rev. Lett.* **80**, 2602 (1998).
- [4] T. Kaneko, Y. Miyahara, R. Hatakeyama and N. Sato, *J. Phys. Soc. Jpn.* **69**, 2060 (2000).
- [5] R.E. Ergun, C.W. Carlson, J.P. McFadden, R.J. Strangeway, M.V. Goldman and D.L. Newman, *Phys. Plasmas* **10**, 454 (2003).
- [6] W.E. Amatucci, D.D. Blackwell, D.N. Walker, G. Gatling and G. Ganguli, *IEEE Trans. Plasma Sci.* **33**, 637 (2005).
- [7] Y. Omura, D. Summers and J. Geophys. Res. **111**, A09222 (2006).
- [8] Y. Kato, Y. Omura and J. Geophys. Res. **109**, A12214 (2004).
- [9] Y. Ueda, M. Tanaka, S. Shinohara and Y. Kawai, *Rev. Sci. Instrum.* **66**, 5423 (1995).
- [10] T. Ono, S. Hiyama, Y. Nakagawa, S. Iizuka and N. Sato, *Plasma Sources Sci. Technol.* **5**, 293 (1996).
- [11] W. Miyazawa, S. Tada, K. Ito, H. Saito, S. Den, Y. Hayashi, Y. Okamoto and Y. Sakamoto, *Plasma Sources Sci. Technol.* **5**, 265 (1996).
- [12] R.D. Tarey, R.K. Jarwal, A. Ganguli and M.K. Akhtar, *Plasma Sources Sci. Technol.* **6**, 189 (1997).
- [13] G. Lisitano, M. Fontanesi and S. Bernabei, *Phys. Rev. Lett.* **26**, 747 (1971).
- [14] J. Musil and F. Zacek, *Plasma Physics* **13**, 471 (1971).
- [15] B. McVey and J. Scharer, *Phys. Rev. Lett.* **31**, 14 (1973).
- [16] R.L. Stenzel, *Phys. Rev. Lett.* **35**, 574 (1975).
- [17] R.L. Stenzel, *Phys. Fluids* **19**, 857 (1976).
- [18] K. Ohkubo and S. Tanaka, *J. Phys. Soc. Jpn.* **41**, 254 (1976).
- [19] H. Sugai, K. Ido, H. Niki, S. Takeda and K. Mima, *J. Phys. Soc. Jpn.* **46**, 1647, (1979).
- [20] A. Ganguli, M.K. Akhtar, R.D. Tarey and R.K. Jarwal, *Phys. Lett. A* **250**, 137 (1998).
- [21] Y. Ueda, H. Muta and Y. Kawai, *Appl. Phys. Lett.* **74**, 1972 (1999).
- [22] A. Ganguli, M.K. Akhtar and R.D. Tarey, *Phys. Plasmas* **5**, 1178 (1998).
- [23] T. Kaneko, H. Murai, R. Hatakeyama and N. Sato, *Phys. Plasmas* **8**, 1455 (2001).
- [24] K. Takahashi, T. Kaneko and R. Hatakeyama, *Trans. Fusion Sci. Technol* **43**, 95 (2003).
- [25] K. Takahashi, T. Kaneko and R. Hatakeyama, *J. Plasma Fusion Res.* **79**, 447 (2003).
- [26] B. Maraghechi, J.E. Willett, H. Mehdian and Y. Aktas, *Phys. Plasmas* **1**, 3181 (1994).
- [27] S. Mirzanejhad and B. Maraghechi, *Phys. Plasmas* **5**, 4070 (1998).
- [28] B. Maraghechi, B. Farrokhi and J.E. Willett, *Phys. Plasmas* **6**, 3778 (1999).
- [29] L. Shenggang, Y. Yang, M. Jie and D.M. Manos, *Phys. Rev. E* **65**, 036411 (2002).
- [30] Y. Amagishi, *Phys. Rev. Lett.* **64**, 1247 (1990).
- [31] M. Inutake, M. Ichimura, H. Hojo, Y. Kimura, R. Katsumata, S. Adachi, Y. Nakashima, A. Itakura, A. Mase and S. Miyoshi, *Phys. Rev. Lett.* **65**, 3397 (1990).
- [32] K. Takahashi, T. Kaneko and R. Hatakeyama, *Phys. Rev. Lett.* **94**, 215001 (2005).
- [33] K. Takahashi, T. Kaneko and R. Hatakeyama, *Phys. Plasmas* **12**, 102107 (2005).
- [34] K. Takahashi, T. Kaneko and R. Hatakeyama, *Phys. Rev. E* **74**, 016405 (2006).
- [35] D.G. Swanson, *Plasma Waves 2nd Edition* (Institute of Physics Publishing, Bristol and Philadelphia, 2003).
- [36] J.D. Kraus, *Antennas* (McGraw-Hill, New York, 1950).
- [37] M. Tanaka, R. Nishimoto, S. Higashi, N. Harada, T. Ohi, A. Komori and Y. Kawai, *J. Phys. Soc. Jpn.* **60**, 1600 (1991).
- [38] H. Shoyama, M. Tanaka, S. Higashi, Y. Kawai and M. Kono, *J. Phys. Soc. Jpn.* **65**, 2860 (1996).
- [39] K. Takahashi, T. Kaneko and R. Hatakeyama, *Appl. Phys. Lett.* **88**, 111503 (2006).
- [40] K. Takahashi, T. Kaneko and R. Hatakeyama, *Plasma Sources Sci. Technol.* **15**, 495 (2006).
- [41] T. Cho, M. Yoshida, J. Kohagura, M. Hirata, T. Numakura, H. Higaki, H. Hojo, M. Ichimura, K. Ishii, K. M. Islam, A. Itakura, I. Katanuma, Y. Nakashima, T. Saito, Y. Tatematsu, M. Yoshikawa, Y. Kojima, S. Tokioka, N. Yokoyama, Y. Tomii, T. Imai, V.P. Pastukhov, S. Miyoshi and Gamma 10 Group, *Phys. Rev. Lett.* **94**, 085002 (2005).
- [42] M. Yoshinuma, M. Inutake, K. Hattori, A. Ando, T. Kaneko, R. Hatakeyama and N. Sato, *J. Plasma Fusion Res. SERIES* **4**, 379 (2001).
- [43] R. Hatakeyama and T. Kaneko, *Phys. Scripta* **T107**, 200 (2004).